Inorganic Chemistry

Article

pubs.acs.org/IC

Rotational Rehybridization and the High Temperature Phase of UC_2

Xiao-Dong Wen,[†] Sven P. Rudin,[†] Enrique R. Batista,[†] David L. Clark,[‡] Gustavo E. Scuseria,[§,∥] and Richard L. Martin*[,†]

[†]Theoretical Division, Los Alamos National Laboratory, Los Alamos, New Mexico 87545, United States

[‡]Los Alamos National Laboratory, Los Alamos, New Mexico 87545, United States

[§]Department of Chemistry, Department of Physics and Astronomy, Rice University, Houston, Texas 77251-1892, United States

[∥]Chemistry Department, Faculty of Science, King Abdulaziz University, Jeddah 21589, Saudi Arabia

Supporting Information

ABSTRACT: The screened hybrid approximation (HSE) of density functional theory (DFT) is used to examine the structural, optical, and electronic properties of the high temperature phase, cubic UC_2. This phase contains C_2 units with a computed C−C distance of 1.443 Å which is in the range of a CC double bond; U is formally 4+, C_2 4−. The closed shell paramagnetic state (NM) was found to lie lowest. Cubic UC_2 is found to be a semiconductor with a narrow gap, 0.4 eV. Interestingly, the C_2 units connecting two uranium sites can rotate freely up to an angle of 30°, indicating a hindered rotational solid. *Ab-initio* molecular dynamic simulations (HSE) show that the rotation of C_2 units in the low temperature phase (tetragonal UC_2) occurs above 2000 K, in good agreement with experiment. The computed energy barrier for the phase transition from tetragonal UC_2 to cubic UC_2 is around 1.30 eV per UC_2. What is fascinating about this system is that at high temperature, the phase transformation to the cubic phase is associated with a rehybridization of the C atoms from sp to sp^3.

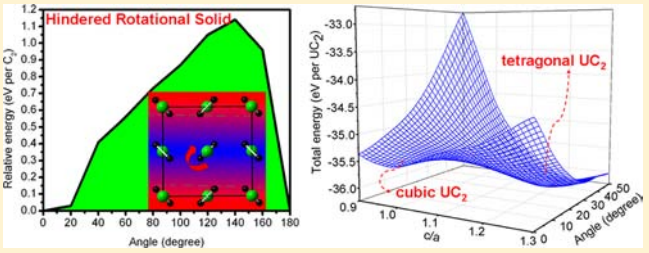

I. INTRODUCTION

C_2 in the gas phase is a simple diatomic molecule which is not very stable, quite unlike the familiar O_2, N_2, and F_2 molecules. However, C_2 anions can be stabilized in solids, and binary metal carbides have long been known. One way to classify these carbides is based on the metal:alkaline-earth metal (A), transition metal (T), and Lanthanide or Actinide metal carbides (LA). The alkaline-earth metal carbides, exemplified by CaC_2, have long been cited in inorganic texts as the simplest example of a salt-like dicarbide. CaC_2 (space group $I4/mmm$) forms in a distorted rock-salt structure with the C_2^{2-} units lying parallel. Notably, the dimeric C−C bond distance is 1.19 Å, typical of an acetylenic triple bond (C_2H_2, 1.20 Å).[1] Most of the binary 4f and 5f metal carbides adopt a CaC_2 (body-centered tetragonal) type structure at room temperature, and can be transformed to a cubic phase at higher temperature.[2] The C−C distance in ThC_2 (1.48 Å), for example, is midway between those typical of double (C_2H_4, 1.34 Å) and single (C_2H_6, 1.54 Å) bonds. This range of C−C from 1.19 Å (in CaC_2) to 1.48 Å (in ThC_2)[3,4] is associated with a range of C_2 reduction from C_2^{2-} (triple bond) when paired with metals which adopt a +2 valence, to C_2^{4-} (double bond) when paired with tetravalent metals such as Th.

In this paper we explore the electronic properties of UC_2. Our initial interest in UC_2 stemmed from its possible use as an advanced nuclear fuel for certain Generation IV reactors such as the gas-cooled fast reactor. Its desirability in this context is associated with its high thermal conductivity and melting point.[5] The desirable thermal conductivity is associated with the fact that it is metallic. This is in contrast to the oxides presently utilized in the nuclear fuel cycle which are insulating. For example, UO_2, is an antiferromagnetically coupled insulator with a gap of 2.1 eV, even though it might be naively expected to possess a partially filled f-band into which each uranium contributes two electrons. The insulating properties are a consequence of strong electronic correlations which act to localize the electrons on individual uranium sites,[6] behavior characteristic of a class of compounds known as Mott insulators. It is important to realize that these correlations favoring localization do not vanish in related materials such as UC_2, they are just not strong enough to drive formation of the energy gap characteristic of an insulator. They behave differently from typical free electron metals and are of fundamental interest in themselves as "strongly correlated metals".

There are two known uranium dicarbide (UC_2) phases. The low temperature, tetragonal phase (space group $I4/mmm$ with a = 3.524 Å and c = 5.999 Å) is isostructural with CaC_2 and remains stable up to 1973 K.[7] The structure of the high temperature phase was initially reported to be cubic, and of either the fluorite (CaF_2) or the pyrite (FeS_2) type.[8,9] It is now firmly established to possess the pyrite structure. Studies by Chang et al.[10] found that a diffusionless phase transformation from the high temperature pyritic to the tetragonal UC_2

Received: May 30, 2012
Published: November 13, 2012

   dx.doi.org/10.1021/ic301133m | *Inorg. Chem.* 2012, 51, 12650−12659

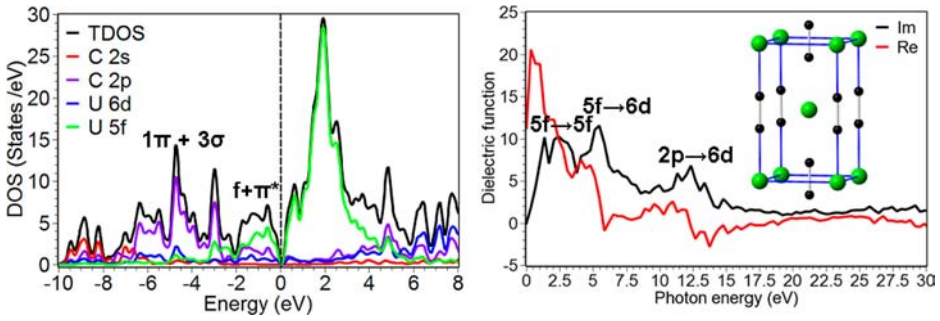

Figure 1. Computed DOS (left) and optical properties (right) of tetragonal UC_2 using HSE, as well as the optimized tetragonal UC_2 structure inserted.

structure takes place in the temperature range 2093 to 2103 K. In addition, neutron diffraction experiments showed that the high temperature phase contains disordered C_2 groups which are either freely rotating, or possess a random orientation along (111).[11] Interestingly, the lattice constant of the high temperature phase is also temperature dependent; for instance, a = 5.41 Å at 2093 K, a = 5.49 Å at 2173 K.

A common feature of the tetragonal and pyritic UC_2 is that there are distinct C_2 pairs isolated from each other in the structures. The structures are qualitatively similar (Figure 1), differing only by a rather small, 25 degree, rotation of the C_2 units about the U−U axis. They are distinguished, however, by quite different bond distances. In the tetragonal ground state, the C−C distance is 1.37 Å. There are two short (2.27 Å) U−C distances and eight long ones (2.58 Å). In the pyritic phase, the uranium atoms now form an fcc lattice, and each uranium is 6-coordinate with U−C bond distances of 2.33 Å. Most interestingly, the C−C distance elongates significantly, from 1.37 Å to 1.44 Å. As we will discuss in more detail later, the phase transition from the tetragonal ground state to the high-temperature cubic structure can be thought of as a tetragonal distortion of the lattice accompanied by a rotation of the C_2 units.

The influence of these rotations on bonding in carbide lattices have captured theorists' attention before. Burdett and McLarnan[12] studied these structures with extended Hückel theory and classified energetic preferences for CaC_2 tetragonal vs pyrite forms as a function of the valence electron count. Long, Hoffmann, and Mayer,[13] also using extended Huckel theory, suggested a low barrier between tetragonal and pyritic phases might be responsible for the spectral broadening observed in the ^{13}C NMR spectra of CaC_2, and proposed a fluxional model for the material. Both of these groups stressed the importance of the increase in metal−carbon bonding associated with the $1\pi_g$ orbital of C_2 in the rotated structure. We note that unlike Ca, uranium adopts a number of oxidation states from U(III) to U(VI), and can therefore be expected to produce a more highly reduced C_2 unit in the tetragonal phase. It is not difficult to imagine even more charge transferred into antibonding orbitals in the cubic phase, accounting for the dramatic increase in the C−C bond length. However, while our calculations predict the structural differences accurately, there is no evidence for additional reduction in the high temperature phase; the ligand remains roughly C_2^{4-}. We argue here that the change in C−C bond length is associated with a rehybridization of the C_2 moiety accompanying the rotation. The ethene-like σ and π orbitals of the ground state change to more ethane-like sp^3 hybrids when the C_2 is rotated.

The organization of this paper is as follows: after a brief introduction to the theoretical approximations employed (section II), we present the total energies, the electronic density of states, band structure, and optical properties of the tetragonal, cubic (pyrite) and (hypothetical) fluorite phases of UC_2 using screened hybrid density functional theory (section III). For comparison, a systematic study of these properties by PBE and PBE + U is also performed, and the results largely presented in the Supporting Information. The connection between the bonding and structural properties and the effect of temperature and pressure on the structure are discussed in section IV, as well as an ab initio molecular dynamics (MD with hybrid functional) description of the phase transition between low and high temperature phases.

II. COMPUTATIONAL METHODS

A first principles predictive capability for strongly correlated materials (typically materials containing partially filled d- or f-shells) has long been problematic and remains one of the grand challenges of electronic structure. A major deficiency of the local density approximation (LDA) and generalized gradient approximation (GGA) is the self-interaction error,[14] which is particularly severe for systems with partially occupied d- or f-states, and causes these approximations to overemphasize the electron delocalization in these materials. Models that add Hubbard U parameters[15,16] (such as LDA +U/GGA+U, where U represents an on-site Coulomb interaction) or alternatives such as hybrid DFT, where the exchange-correlation functional explicitly contains a fraction of the full, nonlocal Hartree−Fock exchange, both remedy the self-interaction problem to some extent, and have met with some success in the Mott insulators. The screened hybrid functionals due to Heyd, Scuseria, and Enzerhof (HSE)[17] have been quite successfully applied to a number of strongly correlated actinide materials and other solids recently,[6,18−24] but to our knowledge have not been applied to the actinide carbides. More recently, the dynamic mean-field theory has been applied to the oxides (AnO_2), nitrides (AnN), and monocarbides (AnC).[25] This approach employs an embedding scheme to map the band structure onto an Anderson impurity model. Its great virtue is that the on-site correlations and multiplet effects can be treated in some detail. It practice, however, it is usually employed in conjunction with an empirical DFT+U band structure and exhibits its associated faults. The great advantage of the hybrid density functional approximations is that, unlike the DFT+U/DMFT approaches, there are no parameters which are changed from one material to another. The parameters in the HSE functional are universal and material independent; that is, the fraction of Hartree−Fock exchange and the screening length which characterize the functional are the same for the H_2 molecule as they are for the UC_2 periodic solid.

Our screened hybrid DFT calculations used the Vienna Ab-initio Simulation Package (VASP)[26,27] using the projected-augmented wave (PAW)[28,29] method to treat the relativisitc core. The U $6s^26p^65f^36d^17s^2$ and C $2s^22p^2$ electrons are explicitly treated as valence

dx.doi.org/10.1021/ic301133m | Inorg. Chem. 2012, 51, 12650−12659

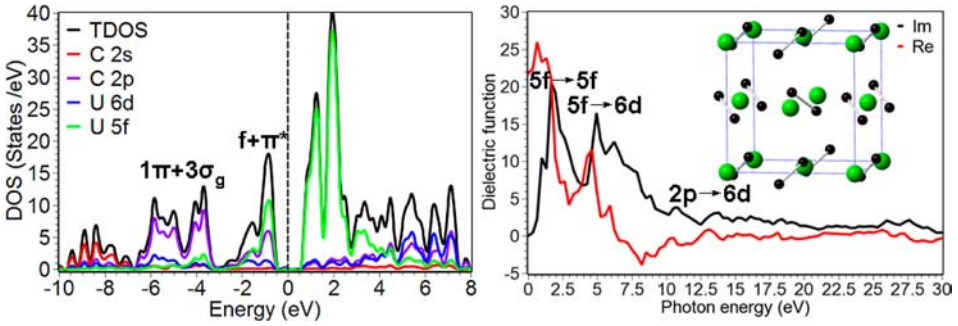

Figure 2. Computed DOS (left) and optical properties (right) of cubic UC_2 using HSE, as well as the optimized cubic UC_2 structure inserted.

electrons. The energy cutoff for the plane-wave basis was set to 500 eV. The Brillouin zone was sampled by Monkhorst−Pack meshes of 15 × 15 × 15 for PBE and PBE + U calculations, 5 × 5 × 5 for HSE calculations because of the computational cost, and a single k point for the MD annealing simulation. Past studies on actinide oxides indicate that the 5 × 5 × 5 grid for HSE is sufficiently accurate for most purposes.[6] Electronic degrees of freedom are considered converged when the total (free) energy change and the band structure energy change between two steps are both smaller than 1×10^{-6} eV. All atoms are fully relaxed until the Hellmann−Feynman forces fall below 0.001 eV/Å. A conjugate-gradient algorithm was used to relax the ions into their instantaneous ground state. We allow all structural parameters (atomic position, lattice constants) to relax. For MD annealing simulation, only the Γ k point was used, with an energy cutoff of 600 eV. A 1 fs time step is utilized. In the HSE calculations, a is set to 1/4 which means HSE contains 25% HF exchange. The screening length, ω is defined as 0.207 $Å^{-1}$ as originally suggested by Heyd et al.[17] The nonspherical contributions[30] from the gradient corrections inside the PAW spheres are considered in current calculations. More details on the HSE can be found in the Supporting Information.

The effect of spin−orbit coupling (SOC)[31] was considered for the antiferromagnetic (AFM), ferromagnetic (FM) and nonmagnetic (NM) initial guesses for cubic UC_2. All three converged to the closed-shell, restricted Kohn−Sham, nonmagnetic solution (NM) for HSE+SOC, as was the case for HSE without SOC. The calculated lattice constants for cubic UC_2 are nearly identical with and without spin−orbit coupling (5.330 Å, HSE+SOC; 5.332 Å, HSE), and the density of states both very similar. Therefore, we discuss only result without SOC in what follows.

III. RESULTS

Three phases of UC_2 are addressed: tetragonal ($I4/mmm$, #139), pyrite (PA-3, #205), and a hypothetical fluorite structure (FM-3M, #225). The tetragonal and fluorite phases are isostructural to CaC_2 and CaF_2, respectively, while pyritic UC_2 exists at high temperatures in the pyrite (FeS_2) structure. At ambient pressure, the HSE calculations predict tetragonal UC_2 to be most stable, followed by the pyrite (+0.80 eV per UC_2) and fluorite structure (+2.30 eV per UC_2). We are principally interested in the pyrite phase because single-crystal quality thin films have recently been synthesized and characterized,[32] but as introduction we will discuss the prediction of hybrid DFT (HSE) for the other phases as well.

Tetragonal Phase. The tetragonal phase of UC_2 is most stable, forming a body-centered system with space group $I4/mm$. Our calculations suggest AFM ordering is preferred over the NM structure by some 0.18 eV per UC_2. The lattice constants (a = 3.515 Å, c = 5.913 Å) computed by HSE for the AFM ordered structure agree reasonably well with experiment (a = 3.524 Å, c = 5.999 Å).[7] Each uranium atom has two short U−C bonds and eight longer U−C bonds. Optimized U−C and C−C distances (in a C_2 unit) are 2.273 Å (2.578 Å) and 1.368 Å. The experimental results are 2.342 Å (2.579 Å) and 1.321 Å, respectively. Each uranium atom has two U−C bonds at 2.273 Å and eight U−C bonds at 2.578 Å. The magnetic moment is computed to be μ = 1.0 μ_B.

The HSE density of states (DOS) and band structure (see Supporting Information) describe tetragonal UC_2 as a poor metal (Figure 1). The results from PBE and PBE+U also both yield metals (see Supporting Information), but with a larger DOS at the Fermi energy. Our results with PBE+U (U = 4.5 eV) agree qualitatively with the calculations on tetragonal UC_2 by Shi et al.[33] who used a value for the Hubbard U of 3.0 eV. As with HSE, the PBE+U results suggest that AFM order lies lowest, although the FM state is nearly degenerate, while PBE yields a nonmagnetic ground state. Thus while qualitatively similar, there are some differences, particularly in the DOS at the Fermi energy, among the three approaches. A high quality photoemission experiment would be welcomed.

This picture emerging from the DOS is echoed in the optical properties. The frequency dependent dielectric matrix[34] allows the determination of optical properties (more details in Supporting Information) Figure 1 (right) shows the HSE dielectric functions with imaginary (black line) and real part (red line) calculated from the frequency dependent dielectric matrix. The dielectric functions indicate once again—through Drude behavior at low frequencies—that the tetragonal UC_2 is a poor metal. The imaginary part of the HSE dielectric function places the first peak around 0.0−2.5 eV which is due to transitions among the U 5f orbitals. The peak situated at around 5−6 eV and 10−12.5 eV can be assigned to the optically allowed U 5f to U 6d and C 2p to U 6d transitions, respectively.

The optical spectra, such as the reflectivity $R(\omega)$, adsorption coefficient $\alpha(\omega)$, energy-loss spectrum $L(\omega)$, refractive index $n(\omega)$, extinction coefficient $K_e(\omega)$ and optical conductivity $\sigma(\omega)$ can be obtained from the dielectric functions, and are given in the Supporting Information.

Pyrite Phase. The HSE energies for pyritic UC_2 show no stabilization associated with magnetic ordering, indicating a nonmagnetic ground state. The optimized lattice constant of 5.332 Å is in fair agreement with the experimental value 5.410 Å at 1820 °C.[11] The computed U−C and C−C distance (in the CC units) are 2.325 Å and 1.443 Å (experimental value 2.330 Å vs 1.460 Å at 1820 °C), respectively. The U−C distance of 2.325 Å is shorter than seen in many structures in the Inorganic Crystal Structure Database (ICSD). These range from ∼2.5 Å to ∼3.3 Å (see Supporting Information). On the other hand, the C−C distance is significantly longer than that in the tetragonal structure, 1.443 vs 1.368 Å. This is at the long end of

dx.doi.org/10.1021/ic301133m | Inorg. Chem. 2012, 51, 12650−12659

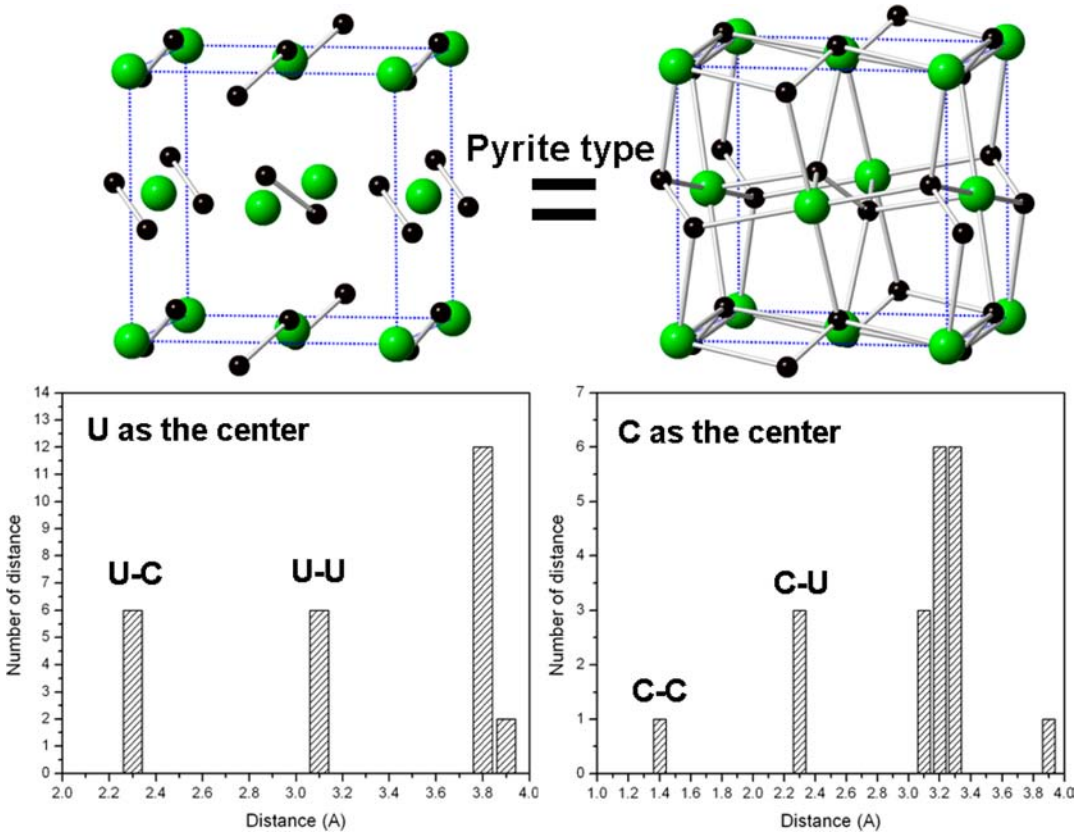

Figure 3. Cubic UC_2 crystal structure and histograms of distances. Black spheres for C atoms; Green spheres for U atoms.

the C−C length distribution in most C_2 containing carbides, which range from 1.19 Å (in CaC_2) to 1.48 Å.[35−37]

Figure 2 (left) shows the different atomic angular momentum contributions to the DOS, the partial density of states (pDOS). From the DOS in Figure 2 (left), one can see that the states from 0 to 3 eV can be assigned to bands of mixed U 5f and C 2p character. The mixing near the Fermi level energy E_f is larger than in the tetragonal ground state, implying a more covalent interaction in the pyrite phase. The C 2p π states are in the range from and 0 to −2 eV and −3 to −7 eV. Above the Fermi level, the unfilled sharp peaks (0−3 eV) are principally U 5f. Thus the gap transition is from a mixed ligand/U5f band to a dominantly U5f band, defining this phase as a ligand-to-metal charge-transfer (LMCT) semiconductor. The U 6d states appear at higher energy, ∼5 eV. The band structure (see Supporting Information) describes a semiconductor with a narrow direct band gap of 0.4 eV at Γ. This band gap was extracted from a numerical tabulation of the gap vs k point, and is slightly different from those inferred from the DOS plots. We were advised by the VASP team that the direct examination of the numerical data is preferred. Both the PBE and PBE+U calculations find cubic UC_2 to be a semiconductor as well (Supporting Information). This would seem to imply a reduced thermal conductivity in the high-temperature phase, but must stand as a prediction until it is experimentally addressed.

Figure 2 (right) shows the imaginary (black line) and real part (red line) of the HSE dielectric function. It indicates—through Drude behavior at low frequencies—that cubic UC_2 is a semiconductor with a narrow gap. The imaginary part of the HSE dielectric function places the first peak around 1.0−2.5 eV which is due to transitions among the U 5f orbitals. The peak situated at around 5−6 eV can be assigned to the optically allowed U 5f to U 6d transitions. The optical spectra obtained from the dielectric functions are given in Supporting Information.

Hypothetical Fluorite Phase. Our HSE calculation suggests that the fluorite UC_2 phase lies significantly higher in energy compared with the tetragonal and cubic phases. The HSE approximation predicts the fluorite phase to be a paramagnetic metal (Supporting Information), with an optimized U−C distance of 2.309 Å. Note that the carbon atoms are now separated by 2.667 Å, indicating no discernible C_2 unit. The U atoms are 8-coordinate, the C atoms 4-coordinate. These bond lengths are consistent with the high energy of the fluorite phase: the strong C−C bond (for a single bond, $D_{298K}{}^0$ = 618 kJ/mol) and the relatively weak U−C bonds ($D_{298K}{}^0$ = 455 kJ/mol) make the system unlike, for example, fluorite UO_2 possessing strong U−O bonds ($D_{298K}{}^0$ = 759 kJ/mol).[38]

IV. DISCUSSIONS

Structural Properties of the Tetragonal and Pyrite Phases. As discussed earlier, the C−C bond length in tetragonal UC_2 is 1.368 Å, indicative of a double bond. In the pyrite phase, the C−C distance elongates significantly to 1.443 Å, a distance lying between ethene, 1.34 Å, and ethane, 1.54 Å, and close to the C−C distances in benzene at 1.40 Å and graphene at 1.42 Å. This is accompanied (see Figure 3) by a tilting of the C_2 units relative to the high-symmetry 001 directions by around 25°. In addition, the U atoms now form an fcc lattice; the histogram of distances suggesting that the U atoms are 6-coordinate (6 U−C bonds at 2.325 Å) and the C atoms 4-fold (1 C−C bond at 1.443 Å and 3 C−U bonds at 2.325 Å). From Figure 4, a histogram of distances in tetragonal

dx.doi.org/10.1021/ic301133m | Inorg. Chem. 2012, 51, 12650−12659

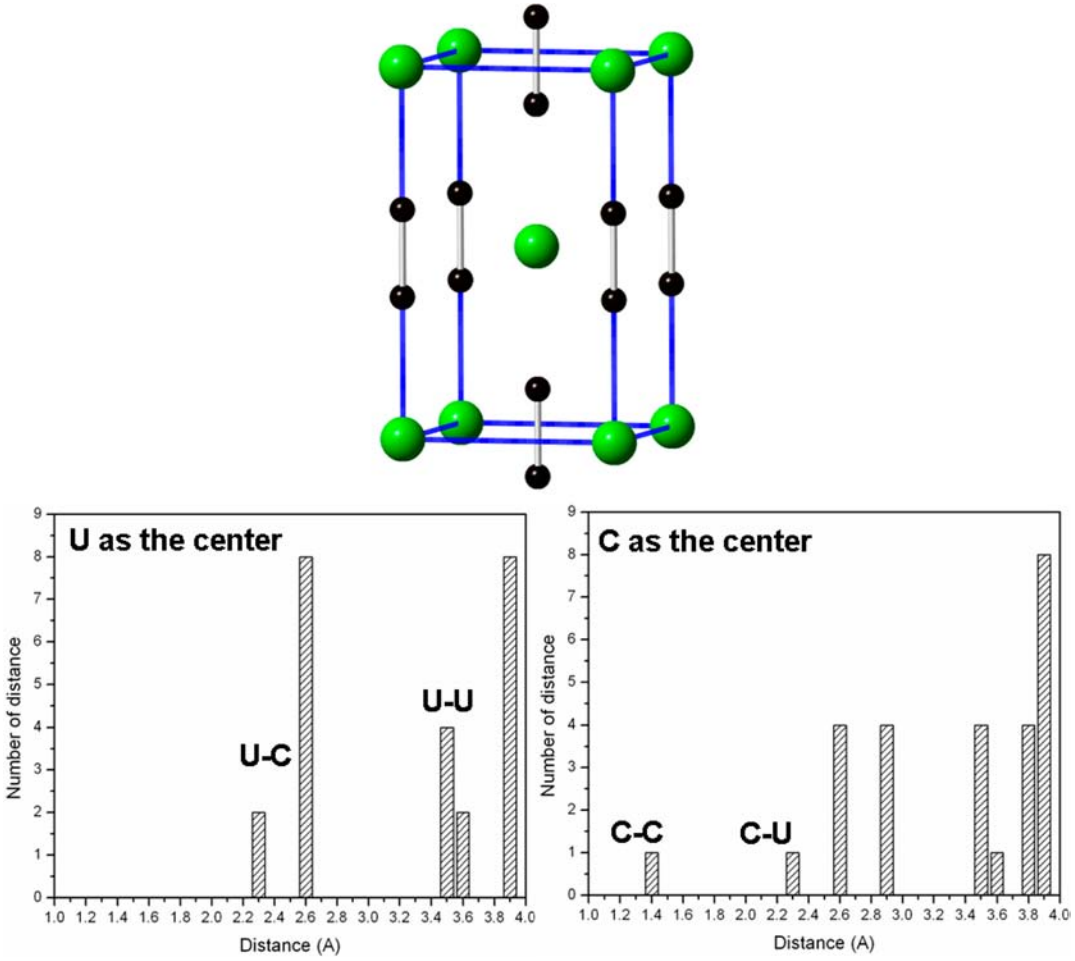

Figure 4. Tetragonal UC_2 crystal structure and the histogram of distance in it.

Scheme 1. Schematic Molecular Orbital Diagram of C_2^{4-} (Left)[a] and Orbital Interaction Diagram for the U^{4+} Cation and C_2^{4-} (Right)[b]

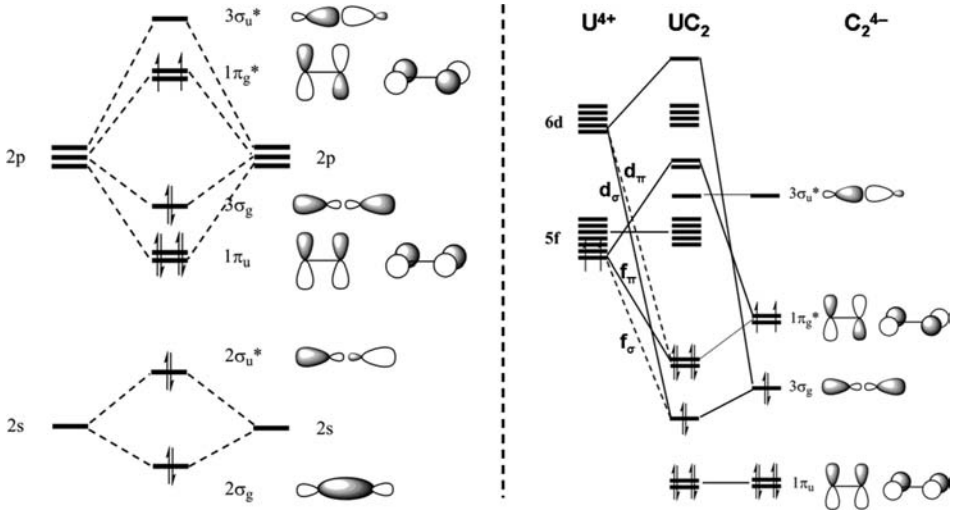

[a]The dashed lines indicated the primary parentage of the orbitals; the 2s-2p mixing is included on the orbital representations of the σ_g and σ_u* orbitals.

[b]Note that because of the end-on arrangement of the U and C_2 units, the inversion symmetry is destroyed, and f-orbitals which are gerade in the free ion, can mix with both gerade and ungerade orbitals in the ligand.

UC_2, one can see that the U atoms are 2 (U−C at 2.273 Å) + 8 (U−C at 2.578 Å) coordinate, and the C atoms are 1 (C−C at 1.368 Å) + 1 (C−U at 2.278 Å) + 4 (C−U at 2.578 Å) coordinate.

dx.doi.org/10.1021/ic301133m | *Inorg. Chem.* 2012, 51, 12650−12659

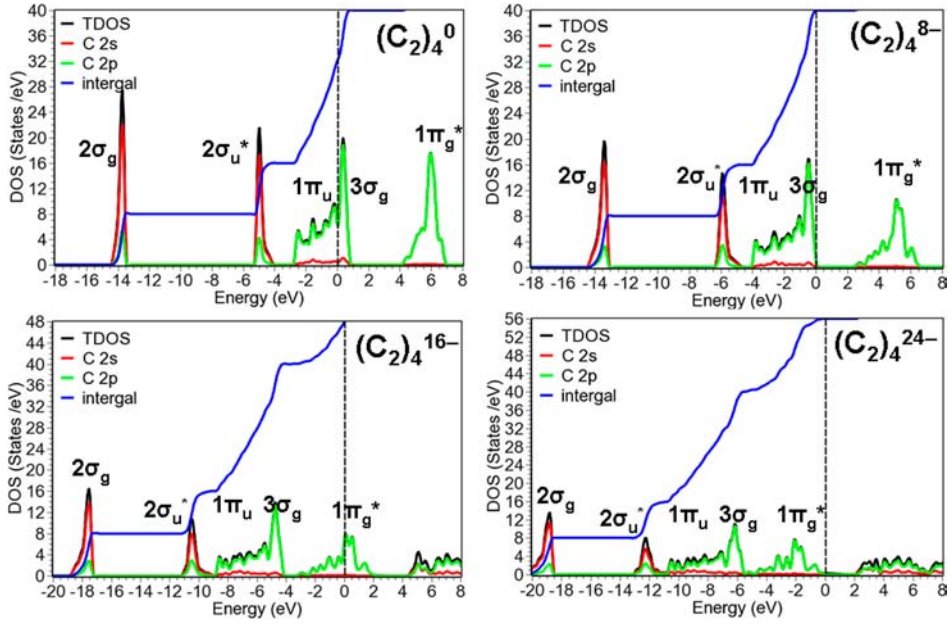

Figure 5. DOS of the isolated carbon sublattice with various charges ($(C_2)_4^{0}$, $(C_2)_4^{8-}$, $(C_2)_4^{16-}$, and $(C_2)_4^{24-}$) in the cubic type. The dotted line indicates the Fermi level. Charge neutrality is achieved by smoothly distributing a neutralizing background positive charge over the unit cell boundary.

If we integrate the components of the partial density of states (pDOS) for tetragonal UC_2, we find a 5f population of ~2.0, signifying a formal U(IV), and implying a C_2^{4-} ligand. From the MO diagram for C_2 shown on the right side of Scheme 1, this would lead to a $1\pi_u^4\ 3\sigma_g^2\ 1\pi_g^{*2}$ configuration. If the $3\sigma_g$ orbital is characterized as bonding, this corresponds to a σ bond and a single net π bond, consistent with an overall double bond and the observed distance. Additional evidence for this comes from a comparison of the pDOS of the UC_2 solid in Figure 1a with that from an identical calculation in which the uranium is removed. Figure 5 shows the expected $1\pi_g^*$ signature (in C_2^{4-}) in the region near the Fermi energy for the C_2^{4-} case. This orbital can also be seen, mixed with U5f, in the pDOS of UC_2 in Figure 1a. We note that many carbides are characterized by C_2^{2-} valences (formal triple bond) with a significantly shorter distance (e.g., CaC_2, R_{CC} = 1.19 Å). Note that calcium is distinguished from uranium in that the former has no d or f orbital available for bonding. As one can see from the right of Scheme 1, empty d_π+d_σ orbitals on the metal can act as electron acceptors from the C_2 $1\pi_u$+$3\sigma_g$ orbitals, and the f_π metal orbitals can back-bond into the $1\pi_g^*$ orbital of C_2, by a simple modification of ideas due to Dewar, Chatt, and Duncanson.[39] Both the σ donation and back bonding into the π^* orbital presumably contribute to the longer C−C bond length observed in UC_2 compared to CaC_2.

The pyrite phase possesses a significantly longer CC distance (1.443 vs 1.368 Å). One would normally associate this increase with an additional transfer of charge to the C_2 unit, further populating the antibonding $1\pi_g^*$ orbital. The similarity of this distance with the benzene bond length suggests another ~0.5 electron donation, leading to a formal bond order of 3/2. This is in line with the observed decrease in metal f orbital population from 2 to 1.85 in the cubic phase, even though it is less than expected for such a large increase in the bond length. However, an increase in the population associated with the π^* orbital in the cubic phase is not observed. In addition, torsion about the U−U axis decreases the overlap between U f_π, d_π orbitals with the $1\pi_g^*$, suggesting a similar or less reduced C_2 unit in the pyrite phase (see the orbital interaction on the right side of Scheme 1). The question, then, is why does the C−C bond length increase so dramatically.

Scheme 2 shows the environment of the C_2 unit in the tetragonal and pyrite forms. Note that the torsion positions C_2 in an "ethane-like" structure in the cubic phase, with the uranium atoms on the face of the cube playing the role of hydrogen atoms. Long, Hoffmann, and Mayer[13] have emphasized that the reduction in symmetry accompanying this rotation allows the C_2 σ and π orbitals to mix, and has a profound effect on the $1\pi_g$ population. The C 2p (1π+$3\sigma_g$) population in pyrite UC_2 is indeed less by 0.3e- than that in tetragonal UC_2, consistent with our view of increased σ donation by C_2 in the cubic phase. This rehybridization also acts to disrupt the C2p bond, thereby increasing the C_2 bond length. On the basis of the calculated DOS in Figure 2 (for tetragonal UC_2) and Figure 1 (for cubic UC_2), the correlation orbital diagram of the C_2 unit in the two phases are plotted, as shown in Scheme 2 (at bottom). One can see that because of the strong U−C interaction in tetragonal UC_2, the $1\pi_u$+$3\sigma_g^*$ broadens, and has a small energy gap with $1\pi_g^*$.

Rotational Properties of the Cubic and Tetragonal Phases. Rotational solids, such as solid H_2,[40] solid CH_4[41] and the C_{60} crystal structure[42] have been known for some time. In these materials, the individual molecular units in the solid can be rotated about their center of mass essentially freely or at least partially so; such rotational behavior is usually associated with molecular crystals. Recently, one of us proposed that solid benzene[43] at pressures below 20 GPa would also be a rotational solid. Given the fact that the C_2 units in the cubic (pyrite type) phase of UC_2 are rotated relative to a collinear U−C−C−U axis, it is interesting to ask about the barrier for rotational motion about this axis, and the possibility that it may exhibit hindered rotational motion. To this end, we consider the rotation of one of the C_2 units about the z axis (in plane) and about the xy diagonal (out of plane). Other rotations encounter

dx.doi.org/10.1021/ic301133m | Inorg. Chem. 2012, 51, 12650−12659

Scheme 2. (Top) Local Coordination Environment of the C−C Fragment in Cubic (a) and Tetragonal (b) UC_2; (Bottom) Correlation Orbital Diagram for a C_2 Unit in the Corresponding Cubic and Tetragonal Geometries

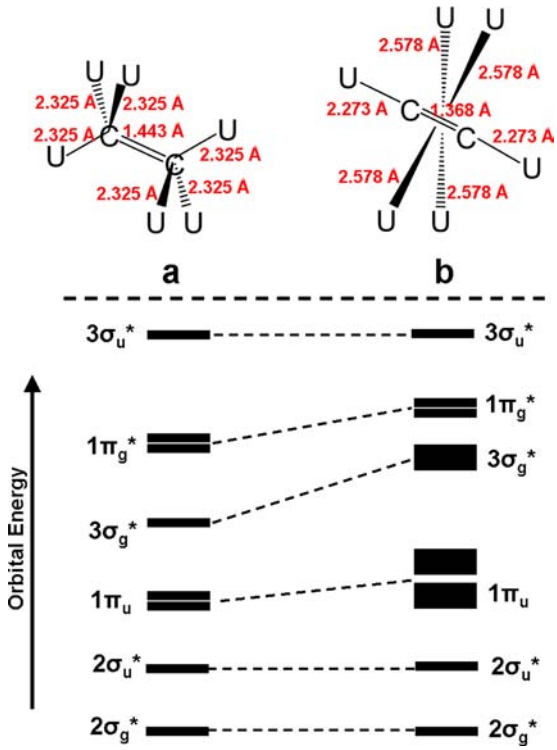

large barriers. The calculations are at ambient pressure and all other atoms are held fixed.

Figure 6a plots the energy surface associated with the two rotations. Rotation about the z axis (energy barrier 1.1 eV per C_2) is substantially easier than rotation about the xy diagonal. However, the barrier is too large to allow free rotation of the C_2 units. On the other hand, the temperature T = 2000 K where the cubic form is observed corresponds to a thermal energy of 0.2 eV. From Figure 6a, rotations through an angle of roughly 30 degrees at $T \approx 2000$ K can be accessed. Above this temperature, the cubic UC_2 phase can be obtained, suggesting that C_2 units might exhibit hindered rotational motion in the cubic phase. We note that the DOS of cubic UC_2 changes little when rotating the C_2 units (see Supporting Information), indicating stable electronic properties. It is not surprising that the application of pressure elevates the rotational barrier (see Supporting Information). Barriers to rotation in the tetragonal ground state are significantly higher, as shown in Figure 6b.

Long, Hoffmann, and Mayer[13] studied, using the extended Hückel method, the distortions in tetragonal $Ca^{2+}(C_2)^{2-}$ and found a low energy barrier (0.1 eV up to 30°) for distortions in which the C_2 dimer rotates into a face of its octahedral Ca environment. The distortion mentioned in their study is associated with the rotation marked by a black dot arrow in the tetragonal UC_2 (Figure 6b). In the current study, one can see there is low energy barrier (0.5 eV) up to 30° and higher energy barrier (4.0 eV) for full rotation.

Transition between Tetragonal and Cubic Phases. DFT computations describe the ground state of the system, that is, the static crystal. To analyze the effect of temperature on the UC_2 phases, we performed NVT (constant particle number,

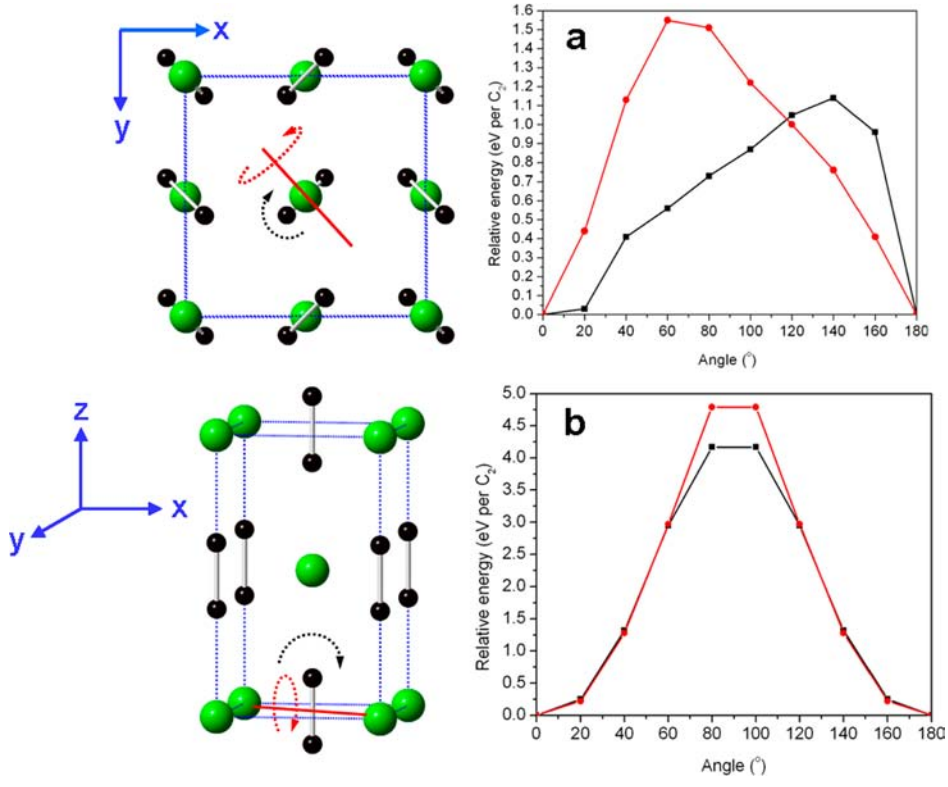

Figure 6. (a) Computed energy barriers (by HSE) for two kinds of rotations of C_2 units in cubic UC_2; (b) computed energy barriers (by HSE) for two kinds of rotations of C_2 units in tetragonal UC_2. The optimized structure at the corresponding pressure is taken as a reference. Only one of the four C_2 units is rotated, as shown on the left; other atoms are held fixed. Black balls represent C atoms; Green balls represent U atoms.

dx.doi.org/10.1021/ic301133m | Inorg. Chem. 2012, 51, 12650−12659

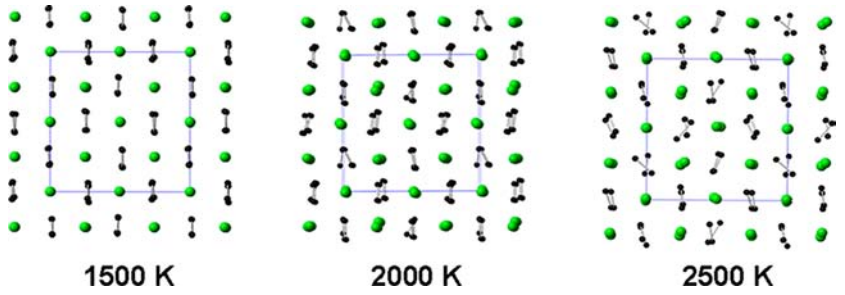

Figure 7. Simulated tetragonal UC_2 phase at 1500, 2000, and 2500 K by ab initio molecular dynamic simulations with the hybrid functional HSE at NVT. Black balls for C atoms; Green balls for U atoms.

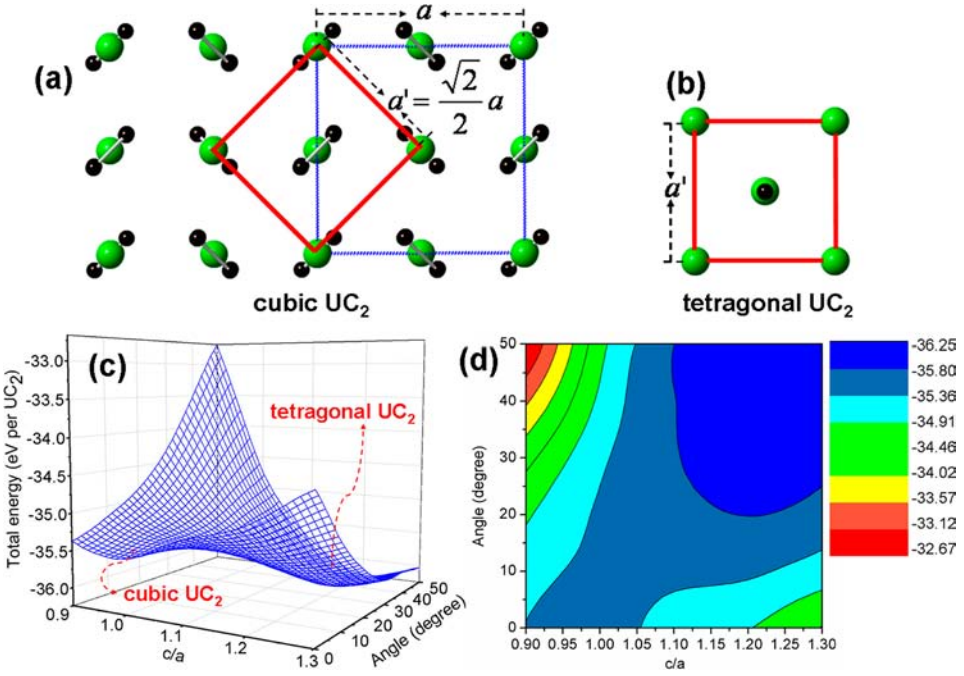

Figure 8. (a) Top view of cubic UC_2 with the tetragonal cell mark by a solid red line; (b) Top view of the tetragonal UC_2; (c) the potential energy surface; (d) a contour representation of the tetragonal to cubic UC_2 phase transition. Black balls represent C atoms; Green balls represent U atoms.

volume and temperature) ab initio molecular dynamic simulations[44] with the HSE hybrid functional. We begin with the 3 × 3 × 3 tetragonal UC_2 phase and simulate dynamics at temperatures of 1500, 2000, and 2500 K, respectively. Representative geometries at these temperatures are shown in Figure 7. Significant rotations of the C_2 units in the tetragonal UC_2 phases occur for temperatures above 2000 K at ambient pressure, in good agreement with experiment.[2]

The barrier between the two phases can be understood by plotting a potential energy surface.[45] Figure 8 (a, b) illustrate the relationship between the crystal structures of tetragonal UC_2 and cubic UC_2; the tetragonal UC_2 structure (with $a' \neq c'$) is identical to the cubic UC_2 structure with $a' = (\sqrt{2}/2)a$, $c' = c$ and the C_2 units along c axis (aligned vertically). In other words, the phase transition from the tetragonal to the cubic UC_2 can be thought of as a tetragonal distortion of the lattice accompanied by a rotation of the C_2 units.

We have studied the energy of the system as a function of the c/a ratio and angle of C_2 rotation (starting from cubic UC_2). The C−C distances also remain fixed at 1.443 Å, characteristic of the cubic phase. Figure 8c shows the potential energy surface as a function of both c/a and the rotation angle. The cubic phase lies ∼1 eV above the low temperature tetragonal phase. The associated barrier from tetragonal to cubic UC_2 is roughly 1.30 eV per UC_2. Note that the barrier for the reverse path is only 0.30 eV per UC_2. The 2D contour in Figure 8d indicates a phase transition path along which both the c/a ratio and the angle of C_2 rotation change smoothly. Given that the calculation is performed at 0 K and ambient pressure, with significant constraints on the degrees of freedom not varied, the actual barrier might be significantly lower.

Under pressure, the tetragonal UC_2 is the most stable phase up to 100 GPa among the three considered UC_2 phases, indicating that the phase transition from the tetragonal to the cubic UC_2 is not pressure-induced (see Supporting Information).

V. CONCLUDING REMARKS

Utilizing the HSE screened hybrid DFT functional, we have investigated the structural, optical, and electronic properties of the room temperature tetragonal, and high temperature cubic phase of UC_2. The cubic phase contains C_2 units with a computed C−C distance of 1.443 Å and is isostructural to Pyrite. HSE predicts that the cubic UC_2 phase is nonmagnetic, a semiconductor with a narrow gap of 0.4 eV. From the f-orbital population, the U is formally 4+ and the C_2 unit 4−, consistent

dx.doi.org/10.1021/ic301133m | Inorg. Chem. 2012, 51, 12650−12659

with the C−C bond length observed experimentally. The cubic UC_2 phase appears to be a hindered rotational solid; the C_2 units can be rotated easily up to an angle of around 30° at the temperatures at which it exists. For the low temperature ground state (tetragonal UC_2), ab initio molecular dynamics simulations with the hybrid functional indicate that the rotation of C_2 units occurs above 2000 K, in good agreement with experiment. A possible path for the phase transition from tetragonal to cubic is explored by computing a constrained potential energy surface. A barrier of 1.30 eV per UC_2 is determined.

It is instructive to compare our results for UC_2 to the closed-shell alkaline earth CaC_2. CaC_2 has no metal orbitals available to interact with the C_2 unit, resulting in an essentially acetylenic C_2^{2-} unit exemplified by its short C−C bond length (1.19 Å) and its σ and π MO parentage observed at all levels of theory. For the related tetragonal phase of UC_2, the availability of multiple oxidation states, and the presence of U 5f and 6d orbitals allows for greater metal−carbon bonding. This occurs as donation of electron density from occupied C_2 MOs into empty U 6d orbitals, and metal back-donation from occupied U 5f orbitals into antibonding C_2 MOs resulting in a C_2 unit most appropriately described as C_2^{4-} with a C−C double bond. What is fascinating about this system is that at high temperature, the phase transformation to the cubic phase is associated with a rehybridization of the C $p\sigma/p\pi$ orbitals to accommodate three sigma bonds to the uranium sites. This reduces the net C−C bonding but maximizes C−U bonding. The latter is reflected in the shortening of the average C−U bonds and the concomitant lengthening of the C−C bond. As a result, the C−C and C−U bond lengths can vary dramatically in the phases of UC_2.

■ ASSOCIATED CONTENT

Supporting Information

(1) Calculated relative energy, lattice constants of the three UC_2 phases using PBE, PBE+U, and HSE; (2) Simulated XRD and Neutron diffraction for the three UC_2 phases; (3) Distance histograms for the three UC_2 phases; (4) Simulated Electron Localization Function (ELF) of the three UC_2 phases; (5) Sublattice analysis of the cubic UC_2; (6) Rotational analysis of the cubic UC_2; (7) Pressure study on UC_2 phases; (8) Effect of screening length (ω) on the electronic and structural properties of the cubic UC_2; (9) Calculated DOS and optical properties for the three UC_2 phases using PBE, PBE+U, and HSE; (10) Mechanical properties of the tetragonal and cubic UC_2 phase. This material is available free of charge via the Internet at http://pubs.acs.org.

■ AUTHOR INFORMATION

Corresponding Author

*E-mail: rlmartin@lanl.gov.

Notes

The authors declare no competing financial interest.

■ ACKNOWLEDGMENTS

Our work at Los Alamos National Laboratory was supported by the Department of Energy Heavy Element Chemistry program and the LDRD program at LANL. X.-D.W. gratefully acknowledges a Seaborg Institute Fellowship. The work at Rice University is supported by DOE, Office of Basic Energy Sciences, Heavy Element Chemistry program under Grant DE-FG02-04ER15523. Some of the calculations were performed on the Chinook computing systems at the Molecular Science Computing Facility in the William R. Wiley Environmental Molecular Sciences Laboratory (EMSL) at PNNL. The Los Alamos National Laboratory is operated by Los Alamos National Security, LLC, for the National Nuclear Security Administration of the U.S. Department of Energy under Contract DE-AC5206NA25396.

■ DEDICATION

Dedicated to Professor Roald Hoffmann on the occasion of his 75th birthday.

■ REFERENCES

(1) Cotton, F. A. *Advanced Inorganic Chemistry*, 4th ed.; John Wiley&Sons: New York, 1980.
(2) McColm, I. J.; Quigley, T. A.; Clark, N. J. *J. Inorg. Nucl. Chem.* **1973**, *35*, 1931−1940.
(3) Jeitschko, W.; Gerss, M. H.; Hoffmann, R.-D.; Lee, S. *J. Less-Common Met.* **1989**, *156*, 397−412.
(4) Li, J.; Hoffmann, R. *Chem. Mater.* **1989**, *1*, 83−101.
(5) Butler, D. *Nature* **2004**, *429*, 238−240.
(6) Wen, X.-D.; Martin, R. L.; Roy, L. E.; Scuseria, G. E.; Rudin, S. P.; Batista, E. R.; McCleskey, T. M.; Scott, B. L.; Bauer, E.; Joyce, J. J.; Durakiewicz, T. *J. Chem. Phys.* **2012**, *137*, 154707.
(7) Rundle, R. E.; Baenziger, N. C.; Wilson, A. S.; McDonald, R. A. *J. Am. Chem. Soc.* **1948**, *70*, 99−105.
(8) Wilson, W. B. *J. Am. Ceram. Soc.* **1960**, *43*, 77−80.
(9) Bredig, M. A. *J. Am. Ceram. Soc.* **1960**, *43*, 493−494.
(10) Chang, R. *Acta Crystallogr.* **1961**, *14*, 1097−1098.
(11) Bowman., A. L.; Arnole, G. P.; Witteman, W. G.; Wallace, T. C.; Nereson, N. G. *Acta Crystallogr.* **1966**, *21*, 670−683.
(12) Burdett, J. K.; McLarnan, T. J. *Inorg. Chem.* **1982**, *21*, 1119−1128.
(13) Long, J. R.; Hoffmann, R.; Meyer, H.-J. *Inorg. Chem.* **1992**, *31*, 1734−1744.
(14) Cohen, A. J.; Mori-Sánchez, P.; Yang, W. *Science* **2008**, *321*, 792−994 , and reference within.
(15) Anisimov, V. I.; Zaanen, J.; Andersen, O. K. *Phys. Rev. B* **1991**, *44*, 943−954.
(16) Anisimov, V. I.; Solovyev, I. V.; Korotin, M. A.; Xzyzyk, M. T.; Sawatzky, G. A. *Phys. Rev. B* **1993**, *48*, 16929−16934.
(17) Heyd, J.; Scuseria, G. E.; Ernzerhof, M. *J. Chem. Phys.* **2003**, *118*, 8207−8215.
(18) Kümmel, S.; Kronik., L. *Rev. Mod. Phys.* **2008**, *80*, 3−60.
(19) Kudin, K. N.; Scuseria, G. E.; Martin, R. L. *Phys. Rev. Lett.* **2002**, *89*, 266402.
(20) Prodan, I. D.; Sordo, J. A.; Kudin, K. N.; Scuseria, G. E.; Martin, R. L. *J. Chem. Phys.* **2005**, *123*, 014703.
(21) Prodan, I. D.; Scuseria, G. E.; Martin, R. L. *Phys. Rev. B* **2006**, *73*, 045104.
(22) Butterfield, M. T.; Durakiewicz, T.; Joyce, J. J.; Prodan, I. D.; Scuseria, G. E.; Guziewicz, E.; Sordo, J. A.; Kudin, K. N.; Martin, R. L.; Arko, A. J.; Graham, K. S.; Moore, D. P.; Morales, L. A. *Surf. Sci.* **2006**, *600*, 1637−1640.
(23) Prodan, I. D.; Scuseria, G. E.; Martin, R. L. *Phys. Rev. B* **2007**, *76*, 033101.
(24) Roy, L. E.; Durakiewicz, T. D.; Martin, R. L.; Peralta, J. R.; Scuseria, G. E.; Olson, C. G.; Joyce, J. J.; Guziewicz, E. *J. Comput. Chem.* **2008**, *29*, 2288−2294.
(25) Yin, Q.; Kutepov, A.; Haule, K.; Kotliar, G.; Savrasov, S. Y.; Pickett, W. E. *Phys. Rev. B* **2011**, *84*, 195111.
(26) (a) Perdew, J. P.; Burke, K.; Ernzerhof, M. *Phys. Rev. Lett.* **1996**, *77*, 3865−3868. (b) Perdew, J. P.; Burke, K.; Ernzerhof, M. *Phys. Rev. Lett.* **1997**, *78*, 1396−1396.
(27) Kresse, G.; Hafner, J. *Phys. Rev. B* **1993**, *47*, 558−561.
(28) Bloechl, P. E. *Phys. Rev. B* **1994**, *50*, 17953−17979.

(29) Kresse, G.; Joubert, D. *Phys. Rev. B* **1999**, *59*, 1758−1775.
(30) See VASP online manual at http://cms.mpi.univie.ac.at/vasp/vasp/LASPH_tag.html.
(31) Kresse, G.; Lebacq, O. VASP manual, http://cms.mpi.univie.ac.at/vasp/.
(32) Private communication with Dr. Thomas M. McCleskey at Los Alamos National Laboratory.
(33) Shi, H.; Zhang, P.; Li, S.-S.; Wang, B.; Sun, B. *J. Nucl. Mater.* **2010**, *396*, 218−222.
(34) Gajdoš, M.; Hummer, K.; Kresse, G.; Furthmüller, J.; Bechstedt, F. *Phys. Rev. B* **2006**, *73*, 045112.
(35) Hoffmann, R. *Am. Sci.* **1995**, *83*, 309−311.
(36) Hoffmann, R. *Am. Sci.* **2002**, *90*, 318−320.
(37) Jeitschko, W.; Gerss, M. H.; Hoffmann, R.-D.; Lee, S. *J. Less-Common Met.* **1989**, *156*, 397−412.
(38) *CRC Handbook of Chemistry and Physics*, 91st ed.; CRC Press: Boca Raton, FL, 2010−2011.
(39) Dewar, M. *Bull. Soc. Chim. Fr.* **1951**, *18*, C71−C79.
(40) Johnson, K. A.; Ashcroft, N. W. *Nature* **2000**, *403*, 632−635.
(41) Huller, M.; Prager, M.; Press, W.; Seydel, T. *J. Chem. Phys.* **2008**, *128*, 034503.
(42) Johnson, R. D.; Yannoni, C. S.; Dorn, H. C.; Salem, J. R.; Bethune, D. S. *Science* **1992**, *255*, 1235−1238.
(43) Wen, X.-D.; Hoffmann, R.; Ashcroft, N. W. *J. Am. Chem. Soc.* **2011**, *133*, 9023−9035.
(44) Car, R.; Parrinello, M. *Phys. Rev. Lett.* **1985**, *55*, 2471−2474.
(45) Wen, X.-D.; Cahill, T. J.; Hoffmann, R. *Chem.—Eur. J.* **2010**, *16*, 6555−6566.